Design of biobased poly(butylene succinate) foams by single-screw extrusion: Identification of relevant rheological parameters controlling foam morphologies

Clément Duborper, Cédric Samuel, André Chateau Akué Asséko, Cyril Loux, Marie-France Lacrampe, Patricia Krawczak

Design of Biobased Poly(Butylene Succinate) Foams by Single-Screw Extrusion: Identification of Relevant Rheological Parameters Controlling Foam Morphologies

C. Duborper,[1,2,3] C. Samuel ,[1,2] A.-C. Akue-Asseko,[1,2,3] C. Loux,[1,2] M.-F. Lacrampe,[1,2] P. Krawczak[1,2]

[1]Ecole Nationale Sup erieure Mines T el ecom Lille Douai (IMT Lille Douai), Department of Polymers and Composites Technology & Mechanical Engineering, 941 rue Charles Bourseul, Douai 59508, France
[2]Universite de Lille, Lille 59000, France
[3]French Institute for Biobased Materials (IFMAS), Parc Scientifique de la Haute Borne, 60 Avenue du Halley, Villeneuve-d'Ascq 59650, France

Key relationships between foam morphologies and melt-state rheological parameters are here exposed for biobased poly(butylene-succinate) (PBS) and standard petrobased polyethylene (PE) foams processed by single-screw extrusion. Scanning electron microscopy followed by image analysis revealed cell diameters and densities in the range of 250–700 mm and 3–4.10^4 cells/cm^3, respec-tively. PBS and PE have similar morphologies except for cell diameters which are slightly higher for PBS foams. The melt index roughly controls foam microstructures but deeper insights are obtained through correlations with shear/extensional rheology experiments. In particular, the melt strength and the strain hardening control the cell growth mechanisms. Concerning the cell density, the shear viscosity in the die plays a key role and agreements with nucleation theories can be discussed based on simu-lated pressure–velocity profiles using finite element soft-ware. In our extrusion conditions, the residence time comes out to have a crucial role with distinct behaviors between PE and PBS indicating a potential modification of the polymer/CO_2 interfacial tension. Consequently, an accurate control of the foam morphology seems achiev-able via a careful selection of the polymer grades and PBS represents a promising alternative to PE for further developments of biobased foams.

INTRODUCTION

For decades, a particular attention was paid within the plastic industry to the development of polymer foams and their related processing by continuous single-screw extrusion processes. Polymer foams historically found numerous applications in packaging and automotive for mechanical shock absorption and various commodity polymers such as polyethylene (PE), polystyrene (PS) or polyurethanes (PU) were used for these purposes [1, 2]. Nowadays, new applications and challenges were found for polymer foams and a rising demand for high-performance foams with specific and controllable properties is clearly observed in transportation, building, electronic and medical markets. In this respect, various properties are actually implemented such as improved biodegradability [3], lower density without sacrificing mechanical strength/rigidity [3–5], lower thermal conductivity/higher thermal insulation [6], improved dielectric properties [7] and/or drug delivery properties [8, 9]. As a consequence, advanced applications of polymer foams require new polymer matrices and an accurate control over the foam morphology in terms of foam density, cell density and cell size and distribution.

Polymer foams are readily obtained by single-screw extrusion processes as a low-cost and continuous production processes. Polyethylene (PE), polypropylene (PP), polycarbonate (PC), acrylonitrile-butadiene-styrene resins (ABS) foams can be extruded using either chemical or physical foaming agents [10]. For the chemical foaming process, endothermic chemical foaming agents (CFA) (sodium bicarbonate and/or citric acid) are now preferred to exothermic CFA such as azodicarbonamide for improved safety and reduced toxicity. Endothermic CFA are usually dry-mixed with polymer pellets before extrusion and, during extrusion, the CFA decomposes into various gases (nitrogen, water, carbon dioxide, etc.) under the action of the shear and the temperature [11]. A homogenous gas/polymer mixture is formed at high pressure in the die and a pressure drop is applied to the polymer/gas mixture at the die exit to induce cell nucleation and growth followed by the solidification of the foamed structure under cooling. Closed-cell foams are mainly produced by single-screw extrusion and extrusion conditions can influence foam morphologies. The die temperature, the flow rate and the CFA concentration can roughly control the expansion ratio and the cell density [12, 13]. However, the pressure drop rate (PDR) in the extrusion die was early identified as a key factor of the cell formation with a specific control over the cell density. The cell density increases with PDR and cells densities ranging from 10^4 to 10^9 cells/cm^3 can be obtained [14, 15] with PDR up to 10 GPa/s. The influence of melt pressure in chemical foaming by extrusion process could be predicted by several nucleation theories where the homogenous polymer/gas phase undergoes a phase separation phenomenon with characteristic nucleation

Correspondence to: C. Samuel; e-mail: cedric.samuel@imt-lille-douai.fr
This study has been granted by the French State under the "Programme d'Investissements d'Avenir" Program supported by the Agence Nationale de la Recherche (ANR, France, contract n°ANR-10-IEED-0004-01) and by the French Institute for Biobased Materials (IFMAS, France). Authors also gratefully acknowledge both the International Campus on Safety and Intermodality in Transportation (CISIT, France), the European Community (FEDER funds) as well as the Hauts-de-France Region (France) for co-funding C. Duborper's PhD grant (contract n°15000305). The authors thank H. Amedro and S. Marcille (Roquette, France) for their support and contribution.
Authors gratefully thank the PMI-2016 organization committee for oral presen-tation acceptance within the Conference on Polymers and Moulds Innovations (PMI-2016), which was held in Ghent (Belgium) 21–23 of September 2016.

TABLE 1. Material designation used in this study with related melt-flow indexes.

Code	Material	Supplier	Grade	MFIa (g/10min)	Melting temperature[a] (°C)
PE1	Low-density polyethylene	Polimeri Europa	Riblene® MR10	20	107
PE2	Low-density polyethylene	ExxonMobil	Exceed 2018CA	2	117
PE3	Linear low-density polyethylene	Polimeri Europa	Flexirene CL10	3	121
PE4	Linear low-density polyethylene	Polyram	Bondyram 4108	1	122
PBS1	Poly(butylene succinate)	Showa Denko	Bionolle 1903MD	5	114
PBS2	Poly(butylene succinate)	Mitsubishi	GSPLA FZ91PD	5	115

Melt flow index—supplier value (190°C, 2.16 kg).
[a]Evaluated by DSC (see Experimental section).

constants depending on various parameters such as temperature, interfacial tension, gas solubility and especially the supersaturation pressure [16, 17]. The homogenous/heterogeneous nature of the cell nucleation also plays a key role. Concerning the cell size, homogeneous foams with cell size ranging from 1 to 500 μm could be obtained and several relationships were previously observed between the rheology of the polymer in the melt state and the resulting cell size. Several authors identified a major effect of the uniaxial extensional viscosity in the melt state on the cell size of PP foams produced by extrusion foaming process [18–20]. However, precise predictive models for any polymers with clear links between rheology–morphology relationships are still unavailable.

Predictive models for polymer foaming by extrusion could be of high interest for the plastic industry and especially for the substitution of petrobased polymers by biobased alternatives. The growing interest in biobased polymers lies in their favorable greenhouse balance and renewability from biomass resources. Combined with equivalent or even superior performances, some of these polymers (PLA, bio-PE, starch-based polymers, etc.) are actually considered as credible alternatives to plastics from fossil resources (PE, PP, etc.) in various applications and their foaming ability attracts a specific attention for potential improvements in terms of foam morphologies. Among biobased polymers, only poly(L-lactide) (PLA) and starch-based plastics have been successfully foamed by extrusion technologies with a moderate control over the foamed morphologies yet [21–23]. A density reduction about 45% has been achieved with PLA with an associate mean diameter and cells density around 100 μm and 10^5 cells/cm^3, respectively. Several other biobased polymers display promising physical properties and especially poly(butylene succinate) (PBS) made from biobased succinic acid [24, 25]. PBS is a biodegradable thermoplastic polyester with a melting temperature (approx. 115–120°C) and mechanical properties close to those of PE or PP (tensile strength 50–70 MPa, elongation at break 100%–150%) [24]. While PLA foaming has been intensively reviewed, the foaming ability of commercially available PBS grades still remains unclear with only a few studies dedicated to PBS foams [26–30]. Most of previous studies were performed in batch/discontinuous conditions [26–29] (i.e., by compression-molding or autoclave) and continuous production of pure PBS foams by extrusion technologies was never reported, expect a PLA/PBS blend incorporating intercalated montmorillonite [30]. However, authors demonstrated the biodegradability of PBS foams [26] and, interestingly, the use of crosslinking agents could reduce the cell size of PBS foams [26], [27] indicating that the melt rheology of PBS could play an important role on its foaming behavior. In this context, the industrial development of biobased/biodegradable PBS foams urgently requires precise guidelines to control PBS foam morphologies (cell diameters, cell densities, size dispersity, etc.) with pilot-scale extrusion equipments.

In this context, this work investigates the foaming ability of biobased PBS grades by single-screw extrusion in the presence of a chemical foaming agent. An industrial extrusion line was used to demonstrate the possibility to substitute polyolefins (especially various PE grades here utilized as standard petrobased polymer foams) by biobased PBS. After morphology analysis of PE and PBS foams, a specific attention is paid to the identification of relevant rheological parameters controlling the cell morphology (cell density, mean cell diameter and the size dispersity). The influence of the pressure drop rate and residence time on the cell density is also studied based on numerical simulations and experimental results.

EXPERIMENTAL

Materials

The polymers investigated in this work are listed in Table 1 with material designation and related melt flow indexes. Two low-density polyethylene (LDPE) grades, two linear low-density polyethylene (LLDPE) grades and two poly(butylene succinate) (PBS) grades were chosen. An endothermic chemical foaming agent (CFA) masterbatch was used (Hydrocerol® ITP848 from Clariant) with a degradation temperature between 160°C and 210°C (corresponding to the thermal degradation range of sodium bicarbonate as the active blowing agent, Supporting Info—Fig. S1).

Foam Processing

Foam processing experiments were carried out on an industrial single-screw extruder (Kaufmann, screw length 840 mm, screw diameter 30 mm) equipped with a static mixer and a specific cylindrical 4-holes die of 4 mm diameter (Fig. 1) at a screw speed of 60 rpm (mass flow rate ranging between 100 and 200 g/min depending on the polymer grade). Extrusion temperatures were set to 120°C, 160°C and 190°C from the hopper to the end of the extruder barrel, to 140°C at the static mixer and to 110°C at the die. All PE and PBS were foamed in the same extrusion conditions (screw speed, barrel and die temperature, CFA concentration) to get reliable information concerning the foaming ability of PBS and the effect of the polymer rheology on the foam morphologies. Prior to extrusion, the CFA was dry-blended with polymer pellets at a concentration of 2wt%. A

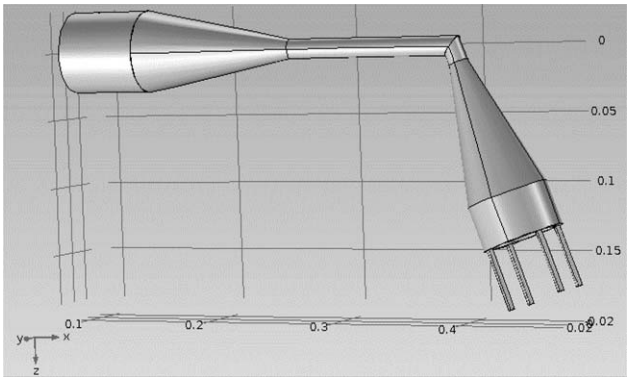

FIG. 1. Schematic representation of the static mixer–die system.

thermocouple/pressure sensor was used to measure the melt temperature (approx. 130°C) and melt pressure at the die entrance.

Characterizations

The cellular morphology of the transverse cross section of the extruded samples previously coated with a thin gold layer (Polaron E5100 series II, Watford) was observed with a scanning electron microscope (SEM, S-4300SE/N, Hitachi, acceleration voltage 5 kV, magnification 35) followed by image treatment using a ImageJ software. Within this study, cells are considered as perfect spheres (in accordance with the as-described process without post-stretching) and the cross-sectional area (A_i) of each individual cell (i) is converted into an equivalent sphere diameter by *Eq. 1*. At least 200 cells are considered for further counting and evaluation of the cell size distribution. Number-average cell diameter (D_n), volume average cell diameter (D_v), cell diameter polydispersity (I_D) and cell density ($\mathcal{C}$) are calculated by *Eqs.* 2–5 [31–33]. The cells size distributions are represented in the form of histogram with an additional fitting with a log-normal function.

$$d_i = (4A_i/\pi)^{0.5} \tag{1}$$

$$D_n = 2\times \frac{\sum n_i \times R_i}{\sum n_i} \tag{2}$$

$$D_v = 2\times \frac{\sum n_i \times R_i^4}{\sum n_i \times R_i^3} \tag{3}$$

$$I_D = \frac{d_v}{d_n} \tag{4}$$

$$\mathcal{C} = \frac{6}{\pi D_n^3} \times \left(1 - \frac{\rho_f}{\rho_p}\right) \tag{5}$$

where n_i is the number of cell having a radius R_i, n is the total cell number; $\mathcal{C}$ is the cell density #/cm^3, ρ_f is the foam density and ρ_p is the polymer density.

Oscillatory shear measurements are performed using an advanced rheometric system (Haake Mars III, ThermoScientific) at desired temperature (ranging from 130°C to 190°C, temperature stabilization time 10 min) under nitrogen atmosphere using plate–plate geometry (diameter 35 mm, gap 0.8 mm). Frequency sweeps from 100 to 0.1 rad s^{-1} were carried out within the linear domain of the materials determined by strain sweeps from 0.01% to 10%. The same rheometer equipped with SER (Sentmanat Extensional Rheometer) test fixture was used to determine the transient extensional viscosities at 130°C at various strain rates between 0.1 and 1 s^{-1}. Transient shear viscosities were also evaluated at 130°C under nitrogen atmosphere using plate–plate geometry (diameter 35 mm, gap 0.8 mm) at a shear rate of 0.1 s^{-1}. Note that the Trouton ratio of 3 was applied to the transient shear viscosity to insure correlations with extensional rheology and identification of the strain-hardening phenomenon. Differential scanning calorimetry (DSC) measurements were performed for each polymer with a Mettler Toledo DSC1 with the following procedure: equilibrate 20°C for 1 min, heating at 40°C/min to 140°C, cooling at 40°C/min to 20°C and heating at 40°C/min to 140°C. The crystallization temperature (T_c) was evaluated at the exothermic peak during the cooling ramp (Supporting Info—Fig. S2). Thermogravimetric analysis of the CFA was carried out on a Mettler Toledo TGA with the following procedure: equilibrate at 20°C for 1 min, heating ramp at 20°C/min up to 700°C.

Numerical Simulations

The commercial FEM (finite element model) software COMSOL Multiphysics was used to obtain simulated temperature, pressure, shear rate and velocities fields inside the extrusion die from experimental entrance melt pressure and temperature. Then, Navier–Stokes/heat transfer equations were resolved in the steady state with die geometry discretized and meshed using free tetrahedral elements. The evolution of the viscosity with shear rate and temperature was also implemented in the FEM software from oscillatory shear experiments by using a Carreau–Arrhenius model (*Eq. 6*) [34, 35].

$$\eta(T,\dot{\gamma}) = \eta_0 \exp\left(i_A \times T\right)\left(1+\lambda+\dot{\gamma}^a\right)^{\frac{m-1}{a}} \tag{6}$$

where λ is the characteristic time (s), m is the pseudoplasticity index, η_0 is the Newtonian viscosity (Pa s), i_A is the Arrhenius index and $a = 2$.

RESULTS AND DISCUSSION

In a first approach, PE and PBS foams display similar densities close to 0.4–0.45 and 0.6 for PE and PBS, respectively (Table 2), representing about 50%–60% decrease in the initial density (PE density = 0.92 and PBS density = 1.26) [36–38]. To get a deeper insight on the cell structure, cross-sectional morphologies of cylindrical foamed extrudates were obtained by SEM (Fig. 2). Note that SEM provided a full analysis of the

TABLE 2. Foam density, cell size, dispersity and cell density for PE and PBS foams.

Material	ρ_{foam} (g/cm^3)	D_v (μm)	D_n (μm)	I_D	Cell density (10^4 cells/cm^3)
PE1	0.42	525	390	1.3	0.8
PE2	0.46	290	165	1.7	4.0
PE3	0.44	400	220	1.8	1.6
PE4	0.43	320	170	1.9	3.2
PBS1	0.59	370	295	1.3	2.1
PBS2	0.63	700	555	1.3	0.3

entire section of the extrudate while only a part of the extrudate is exposed in Fig. 2 for sake of clarity. Extrusion foaming of PE and PBS only produces closed-cell foams and significant differences are observed between all samples in terms of cell size and cell density. Quantitative assessments of the cell density, mean cell diameter and dispersity obtained after image analysis and cell size distributions for each PE and PBS grades are displayed in Fig. 3 and results are gathered in Table 2. Concerning the cell size, the volume mean cell diameter D_v for PE foams can be easily tuned between 290 and 525 μm whereas PBS grades produce foams with higher mean cell diameters in the range of 370–700 μm. Similar trends are also observed with D_n. Concerning the cell density, PE foams can display various cell densities between 0.8 and $4.0.10^4$ cells/cm^3 whereas PBS foams present slightly lower cell densities between 0.3 and $2.1.10^4$ cells/cm^3. Our results are in agreement with high-density polyethylene foams showing cell size close to 400 μm, a void fraction of 50% and cell density close to $1.4.10^4$ cells/cm^3 (similar processing conditions, i.e. single-screw extrusion using sodium bicarbonate as blowing agent) [11]. As a first conclusion, a good foaming ability is noticed for the two PBS grades with a possible tuning and control over the mean cell diameter through an adequate choice of the PBS grades used for extrusion-foaming.

The high fluidity of PE1 with melt flow index (MFI) value close to 20 (Table 1) can explain its peculiar morphology within the LPDE/LLDPE family and its substitution by PBS seems possible. Within the LPDE/LLDPE family, the cell size of PE foams seems to decrease with the MFI value and the MFI value appears as a primary parameter to control the cell diameter in term of D_n. However, deviations are observed on D_v, and the MFI value cannot explain the evolutions observed with the two PBS grades (similar MFI). The melt rheology seems to play a key role with a potential prediction of foam morphologies by quantitative rheological parameters. The cell diameter is governed by cell growth mechanisms after the extrusion die and the

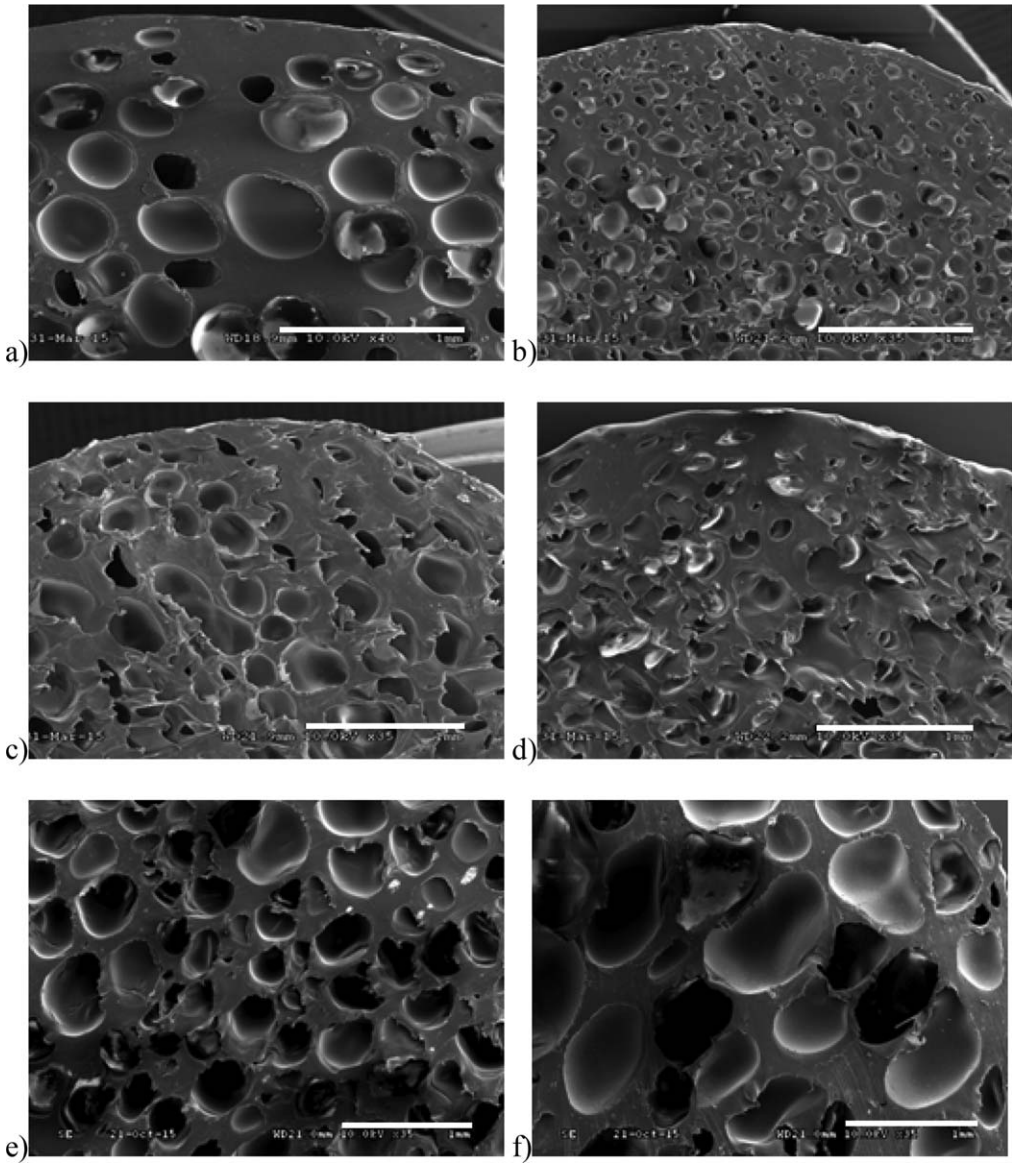

FIG. 2. Morphologies of PE1 (a), PE2 (b), PE3 (c), PE4 (d), PBS1 (e) and PBS2 (f) foams as observed by SEM (scale bar 1 mm).

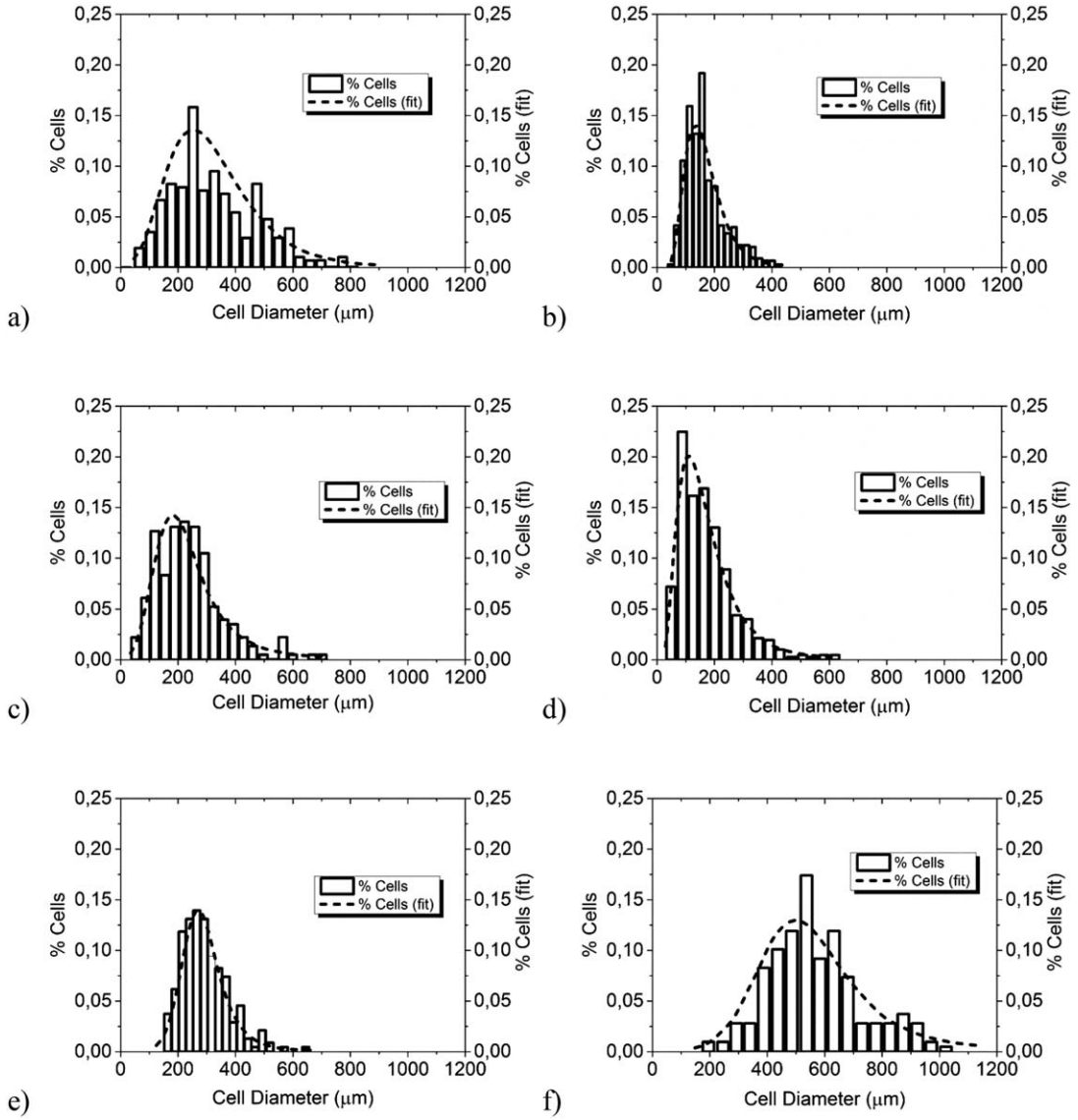

FIG. 3. Cell diameter distribution and the associate log-normal fit for PE1 (a), PE2 (b), PE3 (c), PE4 (d), PBS1 (e) and PBS2 (f).

gas pressure inside the molten polymer cells tends to generate a biaxial stretching of the cell wall [39–41]. In this context, melt-state rheology experiments under extensional stresses are of interest for cell growth mechanisms. Such experiments could be performed with classical dynamic rheometers using specific SER test fixture to apply uniaxial extensional strains/stresses and reach the so-called extensional viscosity. Note that extensional viscosities differ from shear viscosities with (1) a factor 3 (also called the Trouton ratio) between the two values for Newtonian fluids arising from continuity equations of incompressible fluids [42], [43] and (2) potential appearance of a strain-hardening phenomenon marked by rapid increase the extensional viscosity for specific macromolecular architectures [44, 45].

Extensional viscosities as a function of time at various strain rates are displayed in Fig. 4 for all PE and PBS grades (near the melt temperature in the die). The corresponding transient shear viscosity at a low shear rate of 0.1 s^{-1} (multiplied by the Trouton ratio of 3) is also included and fits with transient extensional viscosities for short and intermediate stretching times. Slight discrepancies could be attributed to inherent errors induced by the SER tests [43]. Extensional rheology measurements clearly indicate that PE1 and all PBS grades are subjected to strain-hardening phenomenon with strong to moderate intensity (Table 3). The strain-hardening phenomenon is linked to the presence of long relaxation times arising from long-chain branches on the macromolecular architectures [44, 45]. Our observations consistently agree with previous studies on LDPE/LLDPE [44] and also with the evaluation of the relaxation time spectrum for each polymer grades indicating the presence of long relaxation times (> 0.5 s) for PE1, PE2 and PBS grades. Interestingly, a link is observed between the cell size dispersity and the intensity of the strain-hardening with I_D lower than 1.4 for PE1 and PBS (Table 3). A higher I_D of 1.9 is measured for PE3 and PE4 without strain-hardening (LLDPE) and it can be noticed that PE2 with a poor strain-hardening presents an intermediate I_D of 1.7. In this context, the strain-hardening and the sharp increase

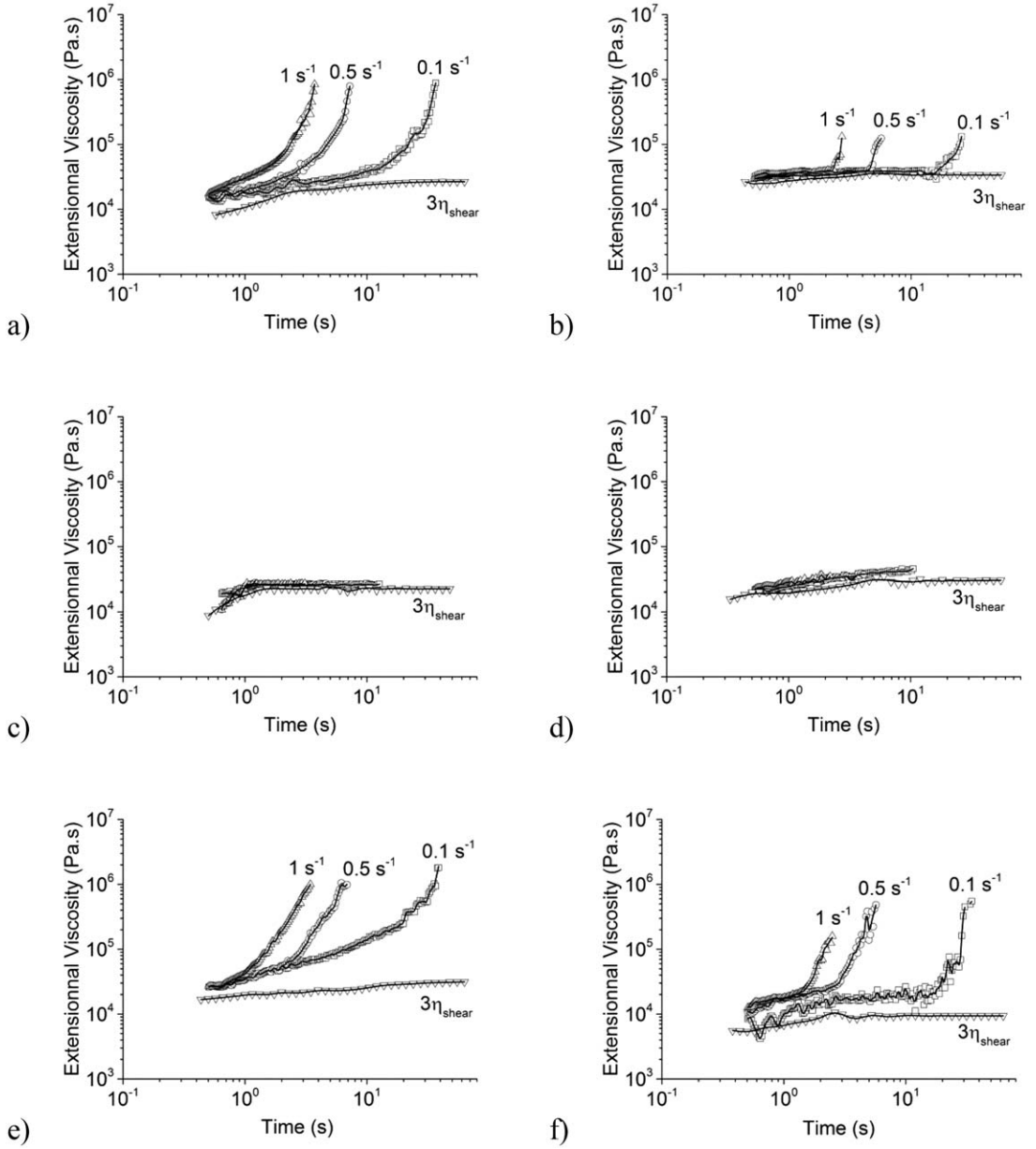

FIG. 4. Extensional viscosity of PE1 (a), PE2 (b), PE3 (c), PE4 (d), PBS1 (e) and PBS2 (f) as a function of stretching time obtained at 130°C with strain rate of 0.1, 0.5 and 1 s^{-1}. Transient shear viscosity (multiplied by the Trouton ratio) is added.

in extensional viscosity can explain the stabilization of the cell size of PE and PBS foams during the growth process outside the extruder. Similar trends are observed for LDPE and PBS with a key role of the macromolecular architecture and the resulting extensional behavior in the melt state on the cell size homogeneity via a stabilization effect, as previously observed on PP foams [20].

The melt fluidity was previously mentioned as a good parameter controlling the cell size of PE and PBS foams and Fig. 4 also shows significant differences between PE and PBS grades in terms of extensional viscosity level that could be linked with melt strength differences at 130°C (close to die temperature). In this context, some rheological parameters are addressed to get a better correlation with cell diameters. In a first attempt, the

TABLE 3. Dynamic, transient shear viscosity and dispersity index for each PE and PBS.

Material	η^*_{die} (Pa s)	η_e^{Tr} (Pa s)	Strain-hardening[a]	T_c (°C)
PE1	570	13,000	Intense	82
PE2	5,200	32,000	Poor	88
PE3	2,930	17,000	None	96
PE4	3,630	21,000	None	91
PBS1	3,710	25,000	Intense	75
PBS2	475	9,400	Intense	75

[a]"Intense" strain-hardening means that extensional viscosity higher than 10^6 Pa s could be reached during strain-hardening at a strain rate of 0.1 s^{-1} (otherwise strain-hardening is "Poor"). "None" means absence of strain-hardening for all strain rates.

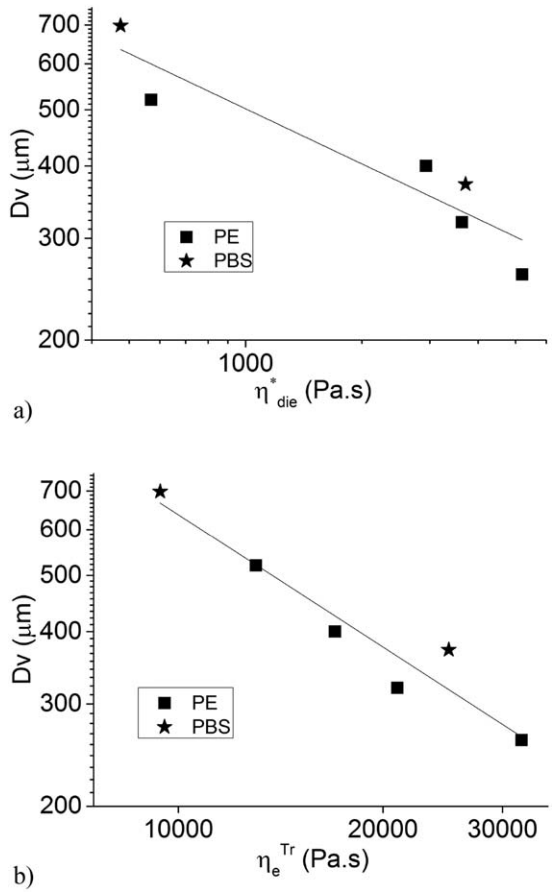

FIG. 5. Evolution of the volume-average cell diameter as a function of the dynamic shear viscosity (a) and the extensional viscosity (b).

dynamic complex viscosity η^*_{die} at a temperature of 130°C and a shear rate of 300 s^{-1} (corresponding to the average shear rate within the extrusion die) is evaluated and listed in Table 3. The volume-average cell diameter D_v as a function of η^*_{die} is displayed in Fig. 5a within a log–log plot and an obvious decrease in the cell diameter is observed with increased η^*_{die}. A power-law relationship is predicted with a slope −0.32 and R^2 of 0.87. Low-viscosity polymers consequently generate larger cell diameter whereas high-viscosity polymers induce low cell diameters. However, the cell growth phenomenon occurs after the die exit according to a biaxial stretching and, in this context, the transient extensional viscosities should be more representative of the cell growth mechanisms. Since the strain rate and the stretching time are both unknown, we here define the transient extensional viscosity at the Troutonian plateau η_e^{Tr}, i.e. the transient extensional viscosity at long stretching time for low strain rates (or the transient extensional viscosity multiplied by 3 for better accuracy). The values are reported in Table 3 and correlations with D_v are displayed in Fig. 5b. A better correlation is obviously obtained by using η_e^{Tr} with a slope −0.75 and R^2 of 0.92. As a conclusion, extensional viscosities and the melt strengths can accurately describe and control the cell growth process and the resultant cell diameter. Note that the growth process occurs in non-isothermal conditions and the crystallization is also investigated (Table 3). Actually, the crystallization temperature during cooling from the melt stat could also play a minor role but no clear trends are observed between PE and PBS grades.

A control over the cell density seems also possible via the selection of polymer grades (Table 2) and the cell density was previously connected by several authors with nucleation process through the pressure drop rate (PDR) in the extrusion die [14]. The effect of PDR in our extrusion conditions was subsequently clarified with a numerical simulation of the pressure–temperature–velocity profiles in the extrusion die. For this purpose, rheological data fitted by a Carreau–Yasuda coupled to Arrhenius model were implemented into the finite element Comsol Multiphysics® software to compute the pressure–temperature–velocity profiles within the die. Figure 6 displays typical evolutions of pressure as a function of the distance from the die entrance for PE1 and PE2. Three distinct zones are observed with their related pressure drops. The first two sections (from $x = 0$ to 13 mm and from $x = 13$ to 22 mm) correspond to the entrance of the die (after the static mixer) where the tube diameter is high and constant, followed by a progressive reduction. The final section before the die exit corresponds to the final contraction with the smallest tube diameter. The highest PDR is observed in this section with ΔP ranging from 4 to 11.5 MPa depending on the PE and PBS grades (Supporting Info—Table S1). The cell nucleation should theoretically occur within this final section [14] and PDR extracted from numerical simulations were found in the range of 1.5–8 MPa s^{-1}. The cell density of all PE and PBS grades was plotted as a function of the PDR (Supporting Info—Fig. S3) but no clear link between the PDR and the cell density is identified, in apparent contradiction with previous works [14, 41] that depicted a positive impact of the PDR on the cell density.

Actually, the homogeneous nucleation theory predicts that the nucleation rate (or the number of nuclei produced per time and volume unit) depends on the gas concentration and various physical parameters such as the polymer/gas interfacial tension and the saturation pressure ΔP_{sat} (*Eq. 7*) [46, 47].

$$J = C_{gas}\ f_H\ \exp\left(\frac{-16\pi\sigma^3}{3kT\Delta P_{sat}{}^2}\right) \tag{7}$$

where J is the nucleation rate (cells/s m^3), C_{gas} is the volume concentration of gas molecules (mol/m^3), f_H a frequency factor, σ is the polymer/gas interfacial tension (N m), k is the

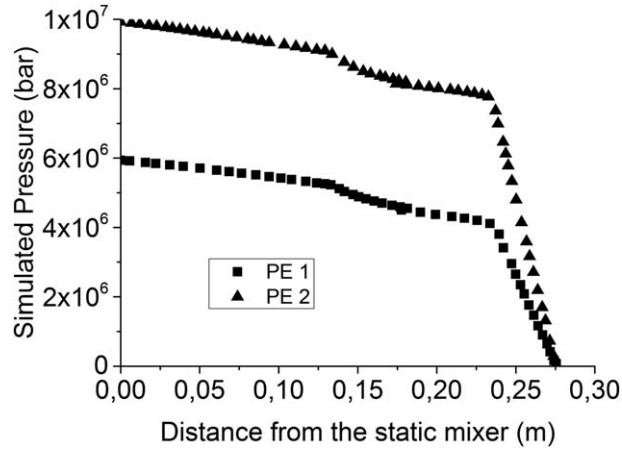

FIG. 6. Simulated pressure profiles within the die for PE1 and PE2.

Boltzmann constant ($1.38.10^{-23}$ kg s/K), T is the melt temperature (K) and ΔP is the supersaturation pressure (Pa).

The classical homogenous theory first implies an instantaneous pressure drop to induce cell nucleation with saturation pressure ΔP_{sat}. The saturation pressure is often described as the difference between the equilibrium pressure P_{eq} and the final pressure. The validity of the classical homogenous theory is here approached and the saturation pressure ΔP_{sat} is assimilated to ΔP_{die} representing the difference between the pressure at the die entrance and the atmospheric pressure (at the die exit). The cell density (or the nuclei density) is subsequently plotted against ΔP_{die} for PE grades (Supporting info—Fig. S4). By assuming an absence of cell/nuclei coalescence and a constant PE/CO_2 interfacial tension within the LDPE/LLDPE family, one should basically predict a positive impact of ΔP_{die} on the cell density. However, no such trend is obviously observed and this finding clearly indicates that our low PDR range induces large difficulties to evaluate various key nucleation parameters and especially the saturation pressure ΔP_{sat} in such dynamic extrusion conditions. The low PDR range also explains our deviations with previous investigations where authors reported PDR in GPa s^{-1} range (approx. 3 decades higher) with cell density close to 10^9 cells/cm^3 [14, 15], [48]. Note that homogenous nucleation probably vanishes and can be replaced by an heterogeneous nucleation phenomenon in these PDR ranges. In spite of the difficulty in getting a reliable value of the saturation pressure, various trends are identified and in particular the effect of the shear viscosity in the extrusion die (η^*_{die}) on the cell density. Note that the shear rate is extracted from the simulated melt velocity and density (approx. 300 s^{-1}). The cell density of PE and PBS foams clearly increases with η^*_{die} (Fig. 7a) and this finding is subsequently connected with the residence time in the extrusion die obtained thought simulated velocity profiles. More surprisingly, a clear linear relationship is found between the residence time and the cell density for PE foams (Fig. 7b). In this respect, the residence time could represent a key factor to tune the cell density of chemically foamed polymers by extrusion and high-viscosity polymers promote cell nucleation due to an enhanced residence time in the die.

To the best of our knowledge, the origin of the linear relationship between the residence time and the cell density still remains experimentally unknown in previous literature and a rationalization of our observed trend is attempted here. Basically, the nucleation rate J obtained through the homogenous/heterogeneous nucleation theory represents the number of nuclei produced per time unit and, by assuming the absence of nuclei/cell coalescence, the cell density or the cell concentration in chemically foamed polymers theoretically increases linearly with the foaming time with respect to *Eq. 8*.

$$\mathcal{C} = J \times t_{foaming} \tag{8}$$

where $\mathcal{C}$ is the cell density (cells/cm^3), J is the nucleation rate (cells/s cm^3) and $t_{foaming}$ is the foaming time (s).

The linear trend observed in Fig. 7b is in agreement with Relation 8 and consequently suggests a constant nucleation rate J within the LDPE/LLDPE family. In this context, it could state out that the saturation pressure ΔP_{sat} representing the thermodynamic driving force for cell nucleation (Relation 7) is nearly similar within the LDPE/LLDPE family. This finding confirms that ΔP_{die} (approx. the pressure at the die entrance) has a minor influence on the nucleation process and suggests that a complex relation between ΔP_{die} and ΔP_{sat}. Indeed, the saturation pressure ΔP_{sat} is often related to the equilibrium pressure P_{eq} obtained from gas solubility data (or Henry's law) and, in dynamic foaming conditions by extrusion at low PDR with a constant gas concentration, the true saturation pressure ($P_{eq} - P$) is probably constant. Regarding the evolution of the cell density with residence time, our data obtained for PBS indicate that the cell density of PBS is more sensitive to the residence time in the die than LDPE/LLDPE (Fig. 7b). An apparent nucleation rate J_{app} is subsequently derived from the slope, 1.1 and $2.2.10^4$ cells/cm^3 s for PE and PBS, respectively. The nucleation rate is consequently enhanced by a factor 2 for PBS compared to LDPE/LLDPE and the origin of this phenomenon could lie in a significant modification of the interfacial tension between CO_2 and the polymer melt as predicted by *Eq. 7*. As a consequence, PBS represents a good candidate to reach a fine control over the cell density by using extrusion equipment. Note also that cell density–residence time plots with subsequent slopes do not pass through the origin, as predicted by *Eq. 8*. This phenomenon could be linked to slight discrepancies between the residence time and the foaming time in the die. The origin is probably linked to a modification of P_{eq} in agreement with gas solubility data for PBS and PE [49–52]. Interfacial tension, gas solubility and residence time effects will be reported in forthcoming investigations based on modified PBS and PE grades to validate our approach of the chemical foaming of polymers by extrusion processes.

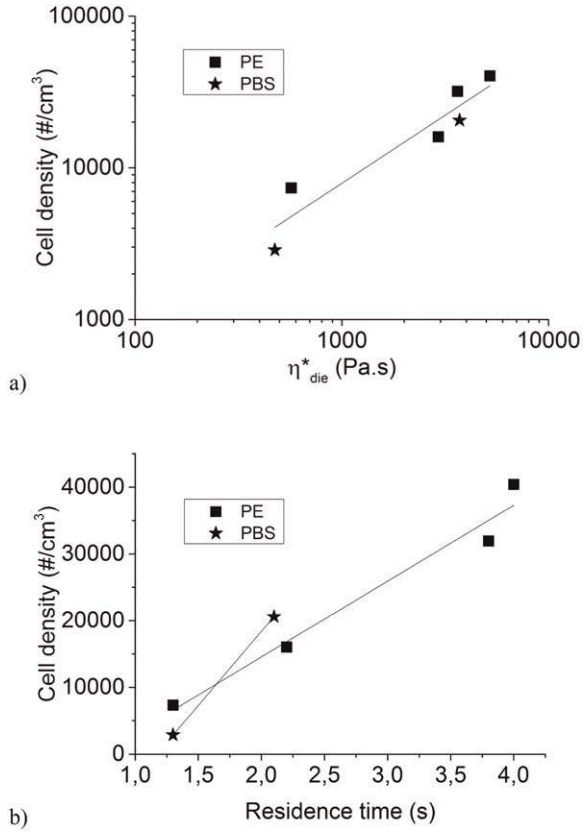

FIG. 7. Evolution of the cell density as a function of the dynamic shear viscosity η^*_{die} for each PE and PBS (a), evolution of the cell density as a function of the residence time in the final section of the die (b).

CONCLUSIONS

Biobased PBS foams were successfully produced by single-screw extrusion using an endothermic chemical blowing agent on an industrial extrusion line. Compared to various standard LDPE/LLDPE grades, PBS foams could present similar morphologies in terms of cell size and density. The influence of melt rheology on foam morphology was clarified and cell sizes/density could be efficiently tuned by the melt viscosity. Low-viscosity polymers tend to induce polymer foams with large cells and low cell density whereas high-viscosity ones displays opposite effects. An accurate control over the cell size could be obtained through the extensional viscosity (or melt strength) as observed by the excellent correlation between the two parameters. However, concerning the cell size homogeneity, linear polymers should be avoided and branched architectures with strain-hardening effects in extensional flows favor a good stabilization of the cell growth. A good control of the cell density was also shown and numerical simulations indicated that cell nucleation probably occurs in the final zone of the die. In the as-reported extrusion conditions, i.e. at low pressure drop rate around 1–10 MPa/s, a high influence of the residence time in the die on the cell density was observed with a quasi-linear relationship. A constant nucleation rate/or saturation pressure for LPDE/LLDPE was found, in agreement with homogeneous/heterogeneous nucleation theories. A higher sensitivity to the residence time was identified for PBS and this effect was attributed to interfacial tension effects between CO_2 and the molten polymer. Forthcoming studies will be dedicated to in-depth quantifications of these phenomenon involving interfacial tension and gas solubility effects in chemical foaming by extrusion. A good potential is consequently observed for biobased PBS in chemical foaming and, based on as-reported observations, an accurate tuning of PBS foam morphology would be possible in the near future by using various modification strategies of commercially available PBS grades.

REFERENCES

1. M. Sauceau, J. Fages, A. Common, C. Nikitine, and E. Rodier, *Prog. Polym. Sci*, **36**, 749 (2011).
2. L.J.M. Jacobs, M.F. Kemmere, and J.T.F. Keurentjes, *Green Chem.*, **10**, 731 (2008).
3. M.E. Gomes, A.S. Ribeiro, P.B. Malafaya, R.L. Reis, and A.M. Cunha, *Biomaterials*, **22**, 883 (2001).
4. S.H. Yetgin, H. Unal, and A. Mimaroglu, *J. Cell. Plast.*, **50**, 563 (2014).
5. V. Dolomanova, J.C.M. Rauhe, L.R. Jensen, R. Pyrz, and A.B. Timmons, *J. Cell. Plast.*, **47**, 81 (2011).
6. A.C. Akué Asséko, B. Cosson, C. Duborper, M.F. Lacrampe, and P. Krawczak, *J. Mater. Sci.*, **51**, 9217 (2016).
7. N. Behrendt, X. Zhang, B. Bergmann, and G.M. Sessler, *Adv. Eng. Mater.*, **10**, 120 (2008).
8. Y. Zhang, J. Zhang, T. Jiang, and S. Wang, *Int. J. Pharm.*, **410**, 118 (2011).
9. C. Wu, Z. Wang, Z. Zhi, T. Jiang, J. Zhang, and S. Wang, *Int. J. Pharm.*, **403**, 162 (2011).
10. C. Okolieocha, D. Raps, K. Subramaniam, and V. Altstädt, *Eur. Polym. J.*, **73**, 500 (2015).
11. Q. Li and L.M. Matuana, *J. Appl. Polym. Sci.*, **88**, 3139 (2003).
12. T. Kuboki, *J. Cell. Plast.*, **50**, 113 (2013).
13. H.E. Naguib, C.B. Park, and N. Reichelt, *J. Appl. Polym. Sci.*, **91**, 2661 (2004).
14. C.B. Park, D.F. Baldwin, and N.A.M.P. Suh, *Polym. Eng. Sci.*, **35**, 432 (1995).
15. S.K. Goel and E.J. Beckman, *Polym. Eng. Sci.*, **34**, 1148 (1994).
16. V. Stralen, *J. Heat Mass Transf.*, **9**, 995 (1966).
17. S.-T. Lee, C.B. Park, and N.S. Ramesh, *Polymeric foams: Science and Technology*, Taylor & Francis CRC Press (2007).
18. N. Najafi, M.-C. Heuzey, P.J. Carreau, D. Therriault, and C.B. Park, *Rheol. Acta*, **53**, 779 (2014).
19. S. Quinn, *Plast. Addit. Compd.*, **3**, 16 (2001).
20. P. Spitael, C.W. Macosko, and S.E.W. Ave, *Polym. Eng. Sci.*, **44**, 2090 (2004).
21. J.M. Julien, J. Bénézet, E. Lafranche, E. Quantin, A. Bergeret, and M.F. Lacrampe, *Polymer*, **53**, 5885 (2012).
22. J.M. Julien, J. Quantin, J. Bénézet, A. Bergeret, M.F. Lacrampe, and P. Krawczak, *Eur. Polym. J.*, **67**, 40 (2015).
23. J.L. Willett and R.L. Shogren, *Polymer*, **43**, 5935 (2002).
24. G. Wang, B. Guo, and R. Li, *J. Appl. Polym. Sci.*, **124**, 1271 (2011).
25. N. Jacquel, F. Freyermouth, F. Fenouillot, A. Rousseau, J.P. Pascault, P. Fuertes, and R. Saint-Loup, *J. Polym. Sci. Part A: Polym. Chem.*, **49**, 5301 (2011).
26. K. Bahari, H. Mitomo, T. Enjoji, F. Yoshii, and K. Makuuchi, *Polym. Degrad. Stab.*, **62**, 551 (1998).
27. S.K. Lim, S.G. Jang, S.I. Lee, K.H. Lee, and I.J. Chin, *Macro Res.*, **16**, 218 (2008).
28. Q. Sun, G.B. Huang, J.H. Ji, and C.A. Zhang, *Adv. Mat. Res.*, **287**, 1805 (2011).
29. S.C. Frerich, *The J. of Super. Fl.*, **96**, 349 (2015).
30. P. Ma, X. Wang, B. Liu, Y. Li, S. Chen, Y. Zhang and G. Xu, *J. Cell. Plast.*, **48**, 191 (2012).
31. L.M. Matuana, O. Faruk, and C. Diaz, *Bioresour. Technol.*, **100**, 5947 (2009).
32. A. Bouzouita, C. Samuel, D. Notta-cuvier, F. Lauro, P. Dubois, and J.M. Raquez, *J. Appl. Polym. Sci.*, **43402**, 1 (2016).
33. R. Gosselin and D. Rodrigue, *Polym. Test.*, **24**, 1027 (2005).
34. Y. Sun and M. Gupta, *Antec*, **49**, 290 (2003).
35. M. Vingaard, B. Endelt, and J. Christiansen, *Proc. 6th Eur. LS-DYNA*, 213 (2007).
36. J. Mejss, *Int. Union Pure Appl. Chem.*, **42**, 552 (1975).
37. T. Fujimaki, *Polym. Degrad. Stab.*, **59**, 209 (1998).
38. S.K. Lim, S.G. Jang, S.I. Lee, K.H. Lee, and I.J. Chin, *Macro. Res.*, **16**, 218 (2008).
39. D. Weaire and R. Phelan, *J. Phys. Condens. Matter*, **8**, 9519 (1999).
40. K.Y. Kim, S.L. Kang, and H.-Y. Kwak, *Polym. Eng. Sci.*, **44**, 1890 (2004).
41. M. Amon and C.D. Denson, *Polym. Eng. Sci.*, **24**, 1026 (1984).
42. V. Tirtaatmadja, *J. Rheol.*, **37**, 1081 (1993).
43. M. Sentmanat, B.N. Wang, and G.H. McKinley, *J. Rheol.*, **49**, 585 (2005).
44. M.H. Wagner, H. Bastian, P. Hachmann, J. Meissner, S. Kurzbeck, H. Munstedt, and F. Langouche, *Rheol. Acta*, **39**, 97 (2000).
45. R. Krishnamoorti and E.P. Giannelis, *Macromolecules*, **30**, 4097 (1997).

46. L.M. Matuana and C.A. Diaz, *Ind. Eng. Chem. Res*., **49**, 2186 (2010).
47. M. Blander and J. Katz, *Adv. Colloid Interface Sci*., **10**, 1 (1975).
48. C.B. Park and L.K. Cheung, *Polym. Eng. Sci*., **37**, 1 (1997).
49. Y. Sato, K. Fujiwara, T. Takikawa, Sumarno, S. Takishima, and H. Masuoka, *Fluid Phase Equilib*., **162**, 261 (1999).
50. Y. Sato, T. Takikawa, A. Sorakubo, S. Takishima, H. Masuoka, and I. Mitsuhiro, *Ind. Eng. Chem. Res*., **39**, 4813 (2000).
51. B. Flaconneche, J. Martin, and M.H. Klopffer, *Oil Gas Sci. Technol*., **56**, 261 (2001).
52. S.H. Mahmood, M. Keshtkar, and C.B. Park, *J. Chem. Thermodyn*., **70**, 13 (2014).